Hydrogenated $Si_{12}Au_{20}$ cluster as a molecular sensor with high performance for NH_3 and NO detection: A first-principle study

Yongliang Yong [a,b], Qingxiao Zhou [a], Xiangying Su [a], Yanmin Kuang [c], C. Richard A. Catlow [b], Xiaohong Li [a]

[a] College of Physics and Engineering, Henan Key Laboratory of Photoelectric Energy Storage Materials and Applications, Henan University of Science and Technology, Luoyang 471023, China
[b] Kathleen Lonsdale Materials Chemistry, Department of Chemistry, University College London, 20 Gordon Street, London WC1H 0AJ, United Kingdom
[c] Institute of Photobiophysics, School of Physics and Electronics, Henan University, Kaifeng 475004, China

a r t i c l e   i n f o

Keywords:
$Si_{12}Au_{20}$ cluster
Hydrogenation
NH_3 and NO sensors
DFT calculations

a b s t r a c t

Using density functional theory (DFT) calculations, we investigated the adsorption of NH_3, NO, CH_4, CO_2, H_2, N_2, H_2O, and O_2 molecules on the (hydrogenated) $Si_{12}Au_{20}$ cluster with the aim of finding a promising molecular sen-sor for NH_3 and NO detection. The $Si_{12}Au_{20}$ cluster could be a disposable molecular sensor for NH_3 and NO be-cause of its long recovery time (over 3 h). To improve the recovery time, we considered the hydrogenation of Si atoms in the $Si_{12}Au_{20}$ cluster to reduce the strength of the adsorption of NH_3 and NO. The vibrational frequency analysis, molecular dynamics simulations and electronic properties show that the $H_{12}Si_{12}Au_{20}$ (HSA) structure is highly stable. NH_3 and NO are chemisorbed on HSA with moderate adsorption energies and evident charge trans-fer, while the other molecules are all physisorbed on HSA. Our results show that the electrical conductivities of HSA will change dramatically due to the adsorption of NH_3 and NO molecules. The recovery time of HSA is pre-dicted to be very short at 300 K. To have a comprehensive comparison with the above results, we also considered different coverages of NO or NH_3 molecules adsorbed on HSA, and the adsorption of NO and NH_3 on the Au_{32} and Si_{32} clusters. We found that Au_{32} and Si_{32} clusters are not suitable for NO and NH_3 detection. We predict that HSA should be a promising gas sensor with high performance for NH_3 and NO detection at low coverage for future ex-perimental validation.

1. Introduction

Intense research has been dedicated to the development of gas sen-sors for detecting and monitoring ultralow concentrations of toxic and harmful gases, which are of concern for safety and sustainable develop-ment. Nitrogen-based gases, such as ammonia (NH_3) and nitrogen monoxide (NO), which are mainly produced by the burning of fossil fuels (including vehicle emissions), chemical production processes, and biomass combustion, have adverse effect on health and cause respi-ratory illness, cardiovascular and immune diseases [1,2]. For example, the Occupational Safety and Health Administration (OSHA) standard for NO gases is given as 25 ppm for 8 h of work shift and 50 ppm for NH_3. Levels over these limits result in severe breathing difficulties, irri-tation to the nose, eyes, skin and throat and even death. Furthermore, NH_3 and NO gases also lead to pollution of water and soil, which results in further harm to plants and aquatic organisms. Therefore, it is of great importance to develop gas sensors with high performance for NH_3 and NO detection.

Recently, research related to gas sensors based on nanoclusters has attracted growing attention owing to their excellent advantages, such as large surface-to-volume ratio, high carrier mobility, and quantum confinement, which directly affect the sensing performances (e.g. sensi-tivity and selectivity) [3–23]. For example, Suematsu et al. [8] have found that Pd-loaded SnO_2 nanoparticle clusters, which were synthe-sized by a hydrothermal method, showed excellent sensitivity to tolu-ene which they were able to detect down to low ppb levels, while Liu et al. [9] have found that the sensor based on Pt activated SnO_2 nanopar-ticle clusters not only has ultrahigh sensitivity, but also possesses good response–recovery properties, linear dependence, repeatability, selec-tivity and long-term stability for NH_3 detection. In particular, metallic nanoclusters have been viewed as promising candidates for gas sensor applications, especially for gold-based nanoclusters [3–6,12,17,21]. However, the physicochemical properties of metallic nanoclusters are found to have strong dependency on the cluster size, geometry, and composition [3]. It is clearly important to understand the characteristics size, geometry, and composition needed for use in gas sensor applica-tions. More importantly, enhancing the gas sensing performance of cluster-based gas sensors is one of the main challenges in the develop-ment of high performance gas sensors. In recent years, the hydrogena-tion strategy has been successfully employed to improve sensing performances of the gas sensors based on metal oxide sensors

[24–27]. The sensing active sites can be modified by the hydrogenation process, which adjusts the adsorption strength and response of gases on the sensors.

Apart from the fundamental understanding of quantum effects such as the finite-size effect, the interest in Si\\Au clusters is primarily based on their applications such as molecular electronic devices, catalyst, gas sensors, etc. [28–41]. There are three main approaches to constructing these clusters: (i) Au doped Si clusters [28–32]: the Au doping process can stabilize particular structures (such as a fullerene-like cage) of Si clusters and lead to unusual properties, such as size selectivity, different charge transfer, large HOMO−LUMO gaps. (ii) Si doped Au clusters [33–37]: the structures of Au clusters can be changed significantly, and the reactivity and catalytic activity of Au clusters affected by Si dop-ing [37]. (iii) mixed Si\\Au clusters [38–41], where very recently, Guo et al. have predicted a very stable configuration of $Si_{12}Au_{20}$ cluster [41] using electronic structure methods. The stability of $Si_{12}Au_{20}$ cluster is verified by vibrational frequency analysis, molecular dynamics simu-lations, and electronic properties such as HOMO-LUMO gap [41]. The hollow, cage-like $Si_{12}Au_{20}$ cluster with I_h symmetry can be viewed as a hollow catalan pentakis dodecahedron, similar to the case of $Cu_{20}Si_{12}$ cluster [42], and may have potential applications in the electronics in-dustry if suitable fabrication process can be developed.

In this work, using computational electronic structure techniques, we investigated the adsorption behaviour and electronic properties of NH_3, NO, CH_4, CO_2, H_2, N_2, O_2, and H_2O molecules on the $Si_{12}Au_{20}$ cluster to study the potential of the $Si_{12}Au_{20}$ cluster in gas sensors for NH_3 and NO detection. Our results show that NH_3, NO, and O_2 molecules are chemisorbed on the $Si_{12}Au_{20}$ cluster with large adsorption energies and charge transfer; however, CH_4, CO_2, H_2, N_2, and H_2O molecules are all physically adsorbed on the cluster. The changes of electronic proper-ties of the $Si_{12}Au_{20}$ cluster, especially for the electric conductivity, are obvious before and after adsorption of NH_3 and NO. However, the strong adsorption of NH_3 and NO on the $Si_{12}Au_{20}$ cluster inhibits desorption which would result in a very long recovery time (over hours). The pure $Si_{12}Au_{20}$ cluster would not therefore be suitable as renewable gas sensors for NH_3 and NO detection, though it has high performance of sensitivity and selectivity. To reduce the strong adsorption of $Si_{12}Au_{20}$ cluster, we then considered the surface modification of the $Si_{12}Au_{20}$ cluster by hydrogenation. Our calculations predict a stable hydroge-nated $Si_{12}Au_{20}$ cluster ($H_{12}Si_{12}Au_{20}$), whose stability was confirmed by vibrational frequency analysis and molecular dynamics simulations. Then the adsorption of NH_3, NO, CH_4, CO_2, H_2, N_2, O_2, and H_2O molecules on the $H_{12}Si_{12}Au_{20}$ cluster was investigated. Our results highlight that the $H_{12}Si_{12}Au_{20}$ is a new promising candidate as a gas sensor with po-tential for high performance (high stability, sensitivity and selectivity, short recovery time) for NH_3 and NO detection. In particular, our results suggest that hydrogenated Si/Au nanoparticles could be effective in the detection of ultralow concentrations of NH_3 and NO.

2. Computational method and details

All calculations in this work have been carried out using spin-polarized density functional theory (DFT) implemented in the $DMol^3$ package (Accelrys Inc.) [43,44]. The exchange-correlation energy func-tional was treated using the generalized gradient approximation (GGA) formulated by Perdew, Burke, and Ernzerhof (PBE) [45] with van der Waals (vdW) correction under the scheme of Tkatchenko and Scheffler [46]. The electron ion-core interactions were represented by density-functional semi-core pseudopotentials fitted to all-electron rel-ativistic DFT results [47] and the standard DNP basis sets. The conver-gence criterion of the energy and electron density was set to 1×10^{-6} Hartree and 1×10^{-6} e/bohr^3 in the self-consistent field calculations, re-spectively. Meanwhile, convergence criteria of 1×10^{-3} Hartree/Bohr on the gradient and displacement and 1×10^{-5} Hartree on the total energy were set in geometrical optimization. The geometric parameters were optimized without symmetry constraints. The charge distributions and

the charge transfer between cluster and molecules were analysed based on Hirshfeld method [48]. Normal-mode frequency vibrational analysis was applied to ensure the structures obtained are real minima; all the configurations presented in this work have no imaginary fre-quencies. Transition state (TS) geometries were firstly searched by using the complete linear/quadratic synchronous transit (LST/QST) method [49], and then fully optimized within the DFT-PBE level. The ab-initio Born-Oppenheimer molecular dynamics (BOMD) simulation was carried out in a NVT ensemble. A Nosé-Hoover chain of thermostats was used to control the temperature.

To evaluate the adsorption strength of molecules on (hydrogenated) $Si_{12}Au_{20}$ cluster, the adsorption energy (E_{ads}) per molecule is defined as

$$E_{ads} = E_{system} - E_{cluster} - nE_{mol} = n; \qquad (1)$$

where E_{system}, $E_{cluster}$ and E_{mol} represents the total energy of the mole-cules adsorbed on the (hydrogenated) $Si_{12}Au_{20}$ cluster, the correspond-ing (hydrogenated) $Si_{12}Au_{20}$ cluster, and the pristine molecule, respectively, and n is the number of molecules.

3. Results and discussion

3.1. Adsorption of molecules on the pure $Si_{12}Au_{20}$ cluster

The pure $Si_{12}Au_{20}$ cluster with I_h symmetry was systematically in-vestigated by Guo et al. [41]. Its configuration is shown in Fig. 1a, and its Cartesian coordinates are shown in Table S1 of Supplementary Infor-mation. Our calculated cohesive energy of the $Si_{12}Au_{20}$ cluster is 3.119 eV per atom, much larger than that of Au_{32} cluster with I_h symme-try (2.338 eV per atom) and Si_{32} cluster (2.331 eV per atom), indicating the greater stability of $Si_{12}Au_{20}$ cluster than Au_{32} and Si_{32} clusters. The HOMO-LUMO gap in present work is 1.038 eV, a little smaller by 0.019 eV than that of Guo et al. [41]. Meanwhile, our calculated cohesive energy is slightly larger than that of 3.069 eV per atom obtained by Guo et al. [41]. These differences are mainly due to the van der Waals (vdW) correction, which is considered in our calculations. The inclusion of the vdW correction generally gives more accurate energies and electronic properties of materials [46]. However, the structure of the $Si_{12}Au_{20}$ clus-ter is the same as predicted in previous work [41], indicating that the vdW correction does not affect the structural properties of the $Si_{12}Au_{20}$ cluster. Although Guo et al. [41] have verified the stability of $Si_{12}Au_{20}$ cluster by vibrational frequency analysis, MD simulations, and electronic structures, to further examine the dynamical stability of $Si_{12}Au_{20}$ cluster, we calculated its phonon dispersion. As shown in Fig. S1a (Supplementary Information), the $Si_{12}Au_{20}$ cluster has no imag-inary frequency, indicating its dynamical stability.

Next, we investigated the adsorption of molecules on the $Si_{12}Au_{20}$ cluster. To obtain the most stable configurations of each adsorbed mol-ecule, we have considered all possible adsorbed configurations. Since the $Si_{12}Au_{20}$ cluster has a high symmetry (I_h), all Au or Si atoms are equivalent. We thus considered two top sites (Si and Au atom), two types of bridge sites (Si\\Au bonds and Au\\Au bonds), and one type of hollow sites (triangle formed by Au-Au-Si) for the adsorption sites. We also considered the orientations of molecules on the adsorption sites. Taking NO molecule as an example, we considered the orienta-tions in which both O and N atoms point to the adsorption sites, and the N\\O bond parallel or vertical to the adsorption sites. After full re-laxation of the several configurations considered, we have obtained the most stable plus a number of low-lying energy structures for each molecule adsorbed on the $Si_{12}Au_{20}$, which are shown in Figs. 1 and 2, while the corresponding calculated results are listed in Tables 1 and 2. To assist the visualisation of the configurations, the cage space is filled by light grey as shown in all the figures presented in the work. It is noted that all the configurations discussed in the subsequent section are found to have no imaginary frequencies, indicating that they are real stable energy minima.
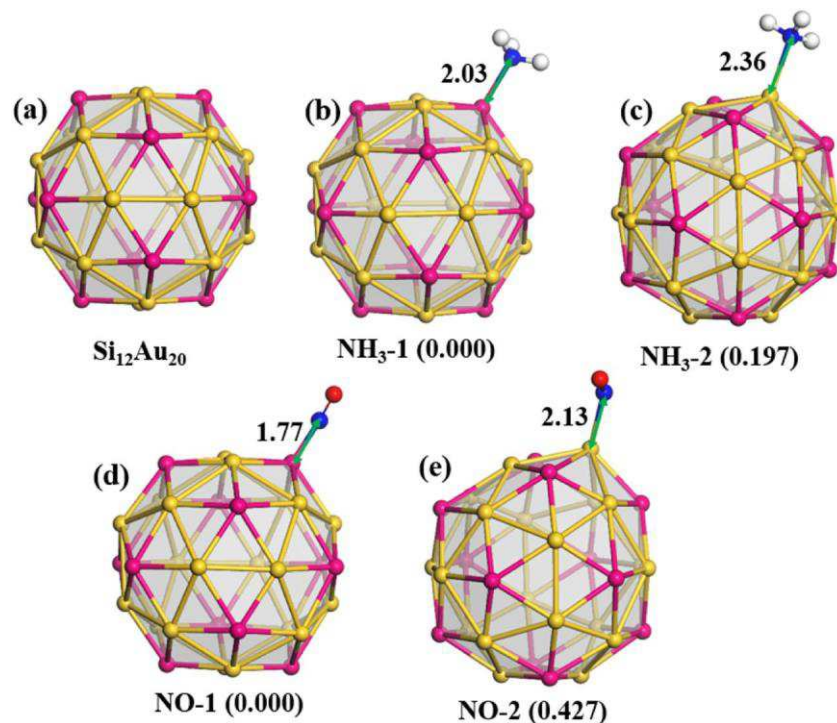
Fig. 1. The optimized structures of $Si_{12}Au_{20}$ cluster without and with gas molecules adsorption: (a) the pure $Si_{12}Au_{20}$ cluster; (b) and (c) NH_3; (d) and (e) NO. Values in parentheses are relative energies with respect to the most stable isomer for each adsorption in eV. The distances between molecules and cluster (shown in green arrowed line) are given in Å. Magenta, yellow, blue, white, and red balls are Si, Au, N, H and O atoms, respectively.

Firstly, we examined the adsorption of NH_3 on the $Si_{12}Au_{20}$ cluster. We found that the most stable configuration of NH_3 on the $Si_{12}Au_{20}$, which is shown in Fig. 1b, is formed by the N atom in NH_3 bonded with one Si atom. This configuration has an adsorption energy of

−0.967 eV. The Si\\N bond lengths of 2.03 Å, is similar to the case of NH_3 adsorbed on silicene [50]. The adsorption energy, bond length, and charge transfer discussed below, indicate that the NH_3 molecule is chemisorbed on the $Si_{12}Au_{20}$ cluster. We also found chemisorption via

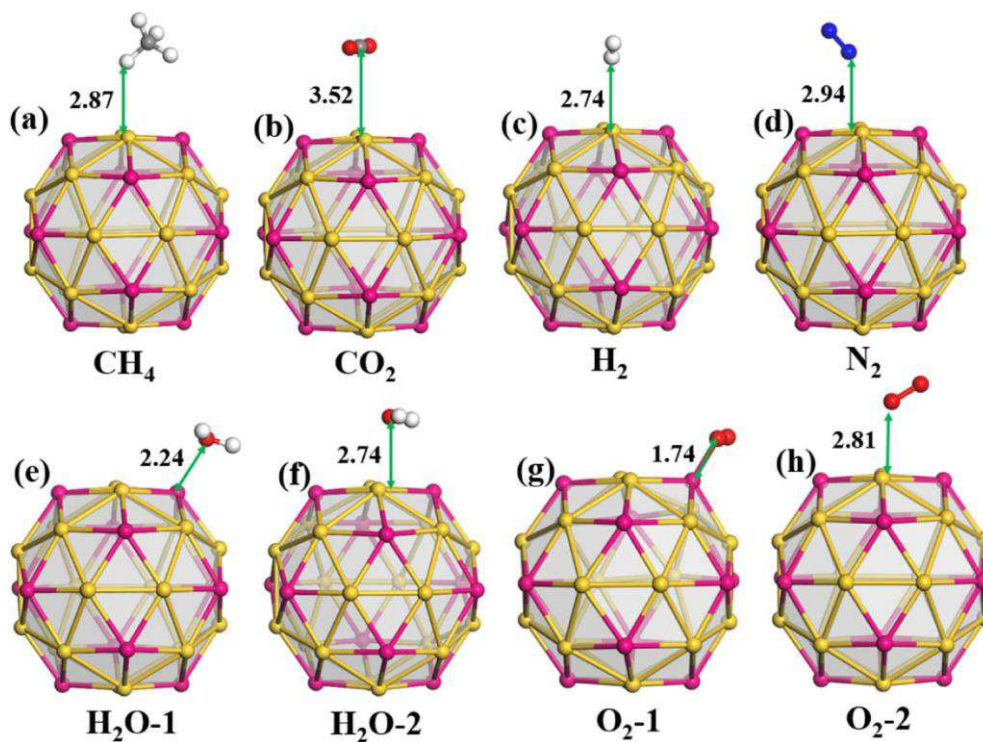Fig. 2. The optimized structures of the $Si_{12}Au_{20}$ cluster with gas molecules adsorption: (a) CH_4; (b) CO_2; (c) H_2; (d) N_2; (e) and (f) H_2O; (g) and (h) O_2. The shortest distances between molecules and cluster (shown in green arrowed line) are given in Å. Grey balls are C atoms.

System	E_{ads} (eV)	E_T (e)	D (Å)	E_g (eV)	τ (s)
NH3-1	−0.967	0.343	2.03	0.997	1.4×10^4
NH3-2	−0.770	0.195	2.36	0.863	7.3
NO-1	−1.058	−0.133	1.77	0.382	4.7×10^5
NO-2	−0.631	−0.064	2.13	0.459	3.5×10^{-2}

the covalent Au\\N bond, which is shown in Fig. 1c, with an adsorption energy of −0.770 eV, which is higher by 0.197 eV than that of the most stable configuration. We note that the adsorption of NH_3 on the cluster via the N\\Au bond leads to some deformation on the cluster, which oc-curs mainly in the region close to the Au atom bonded with the N atom (see Fig. 1c). The average Au\\Au and Au\\Si bond lengths around the adsorption site increase from 2.76 Å and 2.57 Å in pure cluster to 2.83

Å and 2.73 Å, respectively. The deformation electron density as shown in Fig. S2 (Supplementary Information) and the Hirshfeld analysis indi-

cate there is an apparent charge transfer (of at least 0.195 e) from the $Si_{12}Au_{20}$ cluster to the NH_3 molecule (see Table 1), especially for the most stable configuration, indicating that NH_3 serves as an acceptor. Furthermore, the adsorption of NH_3 narrows the HOMO-LUMO gap of the cluster. We see from Table 1 that the HOMO-LUMO gap of isomer NH3-1 and NH3-2 changes from 1.038 eV in the pristine cluster to 0.997 and 0.863 eV, respectively, i.e. a change of 3.95% and 16.9%.

For NO adsorption on the $Si_{12}Au_{20}$ cluster, the NO molecule can chemisorb on the cluster only via the N atom bonding with the cluster, as shown in Fig. 1d–e, as is the case of the NO molecule adsorbed on other Au-based clusters [5,12]. As the most stable configuration as shown in Fig. 1d, the N atom in NO is bonded with Si to form an Si\\N bond with a bond length of 1.77 Å. It has an adsorption energy of −1.058 eV, which is larger than that of NH_3 on the $Si_{12}Au_{20}$ cluster. This may be due to the shorter Si\\N bond in the isomer NO-1 com-pared with that in isomer NH3-1, which leads to much stronger interac-tion in Si\\N bond. Although there is a large adsorption energy, it does not result in any structural deformation for the cluster. When the N

atom in NO interacts with an Au atom, which forms the isomer NO-2 as shown in Fig. 1e, the adsorption energy decreases to −0.631 eV. How-ever, this adsorption induces a substantial structural deformation of the cluster, which is similar to the case of NO molecule adsorbed on Au-based clusters [5,12]. Since the NO molecule can be viewed as an elec-tron donor, some charge (about 0.064–0.133 e) is transferred to the $Si_{12}Au_{20}$ cluster for the two most stable configurations (see the defor-mation electron density as shown in Fig. S2 of Supplementary Informa-

tion). Furthermore, the adsorption of the NO molecule results in a magnetic moment of approximately 1 μ_B, which is similar to the adsorp-tion of NO on other nonmagnetic clusters [5,12–14]. The HOMO-LUMO

gap of isomer NO-1 and NO-2 is 0.382 eV and 0.459 eV, respectively, indicating that there is an obvious change in the HOMO-LUMO gaps after the adsorption of NO, and the change is in the range of 55.8% to 63.2%. Comparing the HOMO−LUMO gaps of NO-cluster complexes with the pristine cluster clarifies the influence of NO adsorption on the electronic properties of the $Si_{12}Au_{20}$ cluster. We found that the adsorption of NH_3 and NO molecules can narrow the HOMO-LUMO gaps, which is because both of molecule adsorption can introduce some impurity states near Fermi level, and unoccupied local states in the unoccupied molecular states as shown in Fig. S3 (Supplemen-tary Information).

We also considered other common gas molecules (CH_4, CO_2, H_2, N_2, H_2O, and O_2) adsorbed on the $Si_{12}Au_{20}$ cluster. Although we explored several initial structures for each molecule on the cluster, we found that they are all physically adsorbed on the $Si_{12}Au_{20}$ cluster with much small adsorption energy and no significant charge transfer except for the H_2O and O_2 molecules. The most stable configuration of each molecule on the cluster is shown in Fig. 2, and the relevant results are listed in Table 2. It can be seen from Table 2 that the physisorption fea-tures for CH_4, CO_2, H_2, and N_2 on the $Si_{12}Au_{20}$ cluster are very evident, and their adsorption does not significantly affect the electronic proper-ties of the $Si_{12}Au_{20}$ cluster. However, in the most stable configuration of H_2O on the $Si_{12}Au_{20}$ cluster, which has an adsorption energy of −0.378 eV, the distance between the O atom and the Si atom is 2.24 Å, which is much larger than the covalent Si\\O bonds of ~1.65 Å in other Si\\O systems [51–53]. There is, however, a significant charge transfer (0.189 e) between the H_2O molecule and the cluster. Therefore, the adsorption of H_2O on the $Si_{12}Au_{20}$ via O interacting has aspects that are intermediate between strong physisorption and chemisorption. However, when the H_2O molecule is close to an Au atom to form the configuration of isomer H_2O-2 as shown in Fig. 2f, the distance between O and Au atom is 2.74 Å, which is similar to the case of H_2O adsorbed on Gd@Au_n (n = 14,15) clusters [12], and indicates a physisorption state for this configuration. The physisorption of CH_4, CO_2, H_2, N_2 and H_2O molecules on $Si_{12}Au_{20}$ cluster just introduces some occupied states, which is located at ᑲ−2.0 eV below the Fermi level, resulting in little in-fluence on the HOMO-LUMO gap (See the Fig. S3 of Supplementary In-formation, where we just showed the DOS of CO_2 and H_2O adsorption due to the similar features of CH_4, H_2, N_2, CO_2 and H_2O). So the electronic properties of the cluster can be affected by the adsorption of these mol-ecules. For the adsorption of O_2 on the $Si_{12}Au_{20}$ cluster, the singlet and triplet states are considered in the spin-polarized calculations. Here we just discussed the ground-state triplet O_2 on the $Si_{12}Au_{20}$ cluster. The most stable configuration as shown in Fig. 2g, in which one O atom in O_2 molecule is bonded with an Si atom to form an Si\\O bond with the length of 1.74 Å, has an E_{ads} of −0.895 eV, accompanied by a charge transfer of 0.277 e from the cluster to O_2 molecule, indicating that the triplet O_2 chemisorbs on the cluster. More importantly, the HOMO-LUMO gap of the cluster narrows to 0.745 eV due to the adsorp-tion of O_2 molecule. However, we found that triplet O_2 only physisorbs on the top of Au atoms (see Fig. 2h). The equilibrium distance of the O_2-cluster is 2.81 Å, with small adsorption energy (−0.126 eV). This weak physisorption hardly affects the electronic properties of the cluster. These results indicate that, if we consider the $Si_{12}Au_{20}$ cluster as gas sen-sors for toxic gas detection, we must prevent the interaction between the H_2O and O_2 molecules and the Si sites in the cluster, as will be discussed below.

3.2. The possibility of the $Si_{12}Au_{20}$ cluster as gas sensors for NO and NH_3 detection

We then explored the possibility of the $Si_{12}Au_{20}$ cluster as a gas sen-sor for NO and NH_3 detection. As a good sensor, it should have excellent performance (sensitivity, selectivity, speed, and stability). The $Si_{12}Au_{20}$ cluster has been confirmed to have high thermodynamic stability by previous work [41]. The sensitivity can be estimated via calculating

System	E_{ads} (eV)	E_T (e)	D (Å)	E_g (eV)
CH4	−0.169	0.051	2.87	1.028
CO2	−0.204	0.027	3.52	1.035
H2	−0.109	−0.041	2.74	1.029
N2	−0.138	−0.002	2.94	1.036
H2O-1	−0.378	0.189	2.24	1.022
H2O-2	−0.345	0.036	2.74	1.000
O2-1	−0.895	−0.277	1.74	0.745
O2-2	−0.139	−0.052	2.81	1.036

the change of electric conductivity (σ) of the $Si_{12}Au_{20}$ cluster before and after adsorption according to the equation:

$$\sigma \propto \exp \frac{-E_g}{2kT} ; \qquad (2)$$

where E_g is the HOMO-LUMO gap value of the configurations, k is the Boltzmann's constant, and T is the thermodynamic temperature. Ac-cording to this equation, the electric conductivity of the $Si_{12}Au_{20}$ cluster at a certain temperature rises by reducing the HOMO-LUMO gap. As discussed above, the HOMO-LUMO gap of the most stable configura-tions of NO (or NH_3) on the $Si_{12}Au_{20}$ cluster significantly decreases, which will lead to a substantial modification of the electric conductivity, indicating that the sensitivity of the $Si_{12}Au_{20}$ cluster for NO (or NH_3) de-tection would be much high.

As discussed above, the CH_4, CO_2, H_2, N_2, and H_2O are all physisorbed on the $Si_{12}Au_{20}$ cluster, and have negligible influence on the electronic properties (mainly conducting properties) of the $Si_{12}Au_{20}$ cluster, how-ever, the adsorption of NO and NH_3 can remarkably change the elec-tronic properties of the cluster (i.e. a large change in the HOMO-LUMO gap before and after adsorption is found). Therefore, the $Si_{12}Au_{20}$-based gas sensor is predicted to show high selectivity for NH_3 and NO detection compared with CH_4, CO_2, H_2, N_2, and H_2O, which should be similar to the case of B_{40}-based gas sensor [15]. Using the non-equilibrium Greens function (NEGF) method, Lin et al. have predicted high sensitivity and selectivity for the B_{40} fullerene-based sensor for NH_3 detection in comparison with H_2, N_2 and CH_4 [15]. Another impor-tant parameter of gas sensor is speed, i.e. the response and recovery rate. However, it is difficult to evaluate the response time due to the lack of knowledge of several parameters. In the present work, we at-tempt crudely to estimate the recovery time (τ) based on transition state theory, applied to the rate of desorption:

$$\tau = \upsilon_0^{-1} \exp \frac{-E_{ads}}{kT} ; \qquad (3)$$

where υ_0 is the attempt frequency, E_{ads} is the adsorption energy as de-fined in Eq. (1). The adsorption energies (−0.34 ~ −0.79 eV) and recovery times (0.5 μs ~ 16 s) from previous theoretical calculations on NO_2 adsorbed on carbon nanotubes are remarkably smaller and shorter than the corresponding experimental results [54]. Peng et al. suggested that when NO_2 molecules experimentally interact with the carbon nanotubes, a reaction occurs to produce to NO and NO_3 molecules. NO and NO_2 have fast recovery time (≤1 s at room temperature), while NO_3 has longer ones (12 h), and the NO_3 concentration is major on the nanotube surface. So they deduce that NO_3 is responsible for the slow recovery [54]. Thus, we can successfully explain the reason why the experimental recovery time has been measured to be long or short by using the theory mentioned above. If we assume that the attempt fre-quencies of all the considered molecules have the same value as that for the NO_2 molecule (10^{12} s^{-1}) [54], the calculated recovery times at T = 300 K are listed in Table 1. We find that when the N atom is bonded with Si to form the most stable configuration of NH_3 or NO on the $Si_{12}Au_{20}$ cluster, the estimated recovery times for NH_3 and NO are 3.95 h and 130.7 h, respectively, which is too long to allow the reuse of $Si_{12}Au_{20}$-based sensor. Furthermore, the interaction between O_2 and the $Si_{12}Au_{20}$ cluster, with important implications for the stability of the cluster upon air exposure, is so strong that it may hinder the ap-plications of the cluster as chemical sensors. When these results (ad-sorption energy, charge transfer, thermodynamic stability, high sensitivity and selectivity, and recovery time) are considered together, the $Si_{12}Au_{20}$ sensor is predicted to have high sensitivity and selectivity, but poor performance as to recovery time; thus, the $Si_{12}Au_{20}$ sensor could only be used as a disposable molecular sensor for NH_3 or NO detection.

3.3. The structure and stability of the $H_{12}Si_{12}Au_{20}$ cluster

It is clear that the strength of the adsorption of NH_3 and NO and the consequent slow recovery times is the main challenge for developing $Si_{12}Au_{20}$-based sensors. As discussed above, we found that the most sta-ble configurations of NH_3 and NO on the $Si_{12}Au_{20}$ cluster, which have the biggest adsorption energy, are always formed by the molecule (NH_3 and NO) interacting with the Si atoms; however, the configura-tions that are formed by the molecule interacting with the Au atoms have moderate adsorption energy, which corresponds to a much shorter recovery time (see Table 1). Moreover, the adsorption energy of H_2O and O_2 on the $Si_{12}Au_{20}$ cluster is a little stronger. Thus, preventing the interaction between H_2O and O_2 molecules and the Si sites would de-crease the adsorption strength and hence the recovery time. Previous work has demonstrated that the hydrogenation strategy can be success-fully employed to improve sensing performances of the gas sensors [24–27]. Moreover, hydrogenated Si-based clusters are stable because of the hydrogen termination of the dangling bonds of each Si, which hinders interaction with surrounding materials [55–59]. Therefore, we considered the hydrogenated $Si_{12}Au_{20}$ cluster, hydrogenating the Si atoms in the clusters, i.e. $H_{12}Si_{12}Au_{20}$ (so-called HSA).

To investigate the hydrogenation of the cluster, we first adsorbed a single H atom on the $Si_{12}Au_{20}$ cluster. We found that the H atom can bond with Au and Si atom to form stable configurations, which are shown in Fig. 3A and B, respectively. The adsorption energies of the H atom on Si and Au are −2.526 eV and − 1.938 eV, respectively, indicating the formation of Si\\H bond is significantly more energetically favourable, as are the cases of NH_3 and NO on the cluster. To discuss fur-ther the adsorption behaviour of H on the $Si_{12}Au_{20}$ cluster, the transition state (TS) between structure A formed by H bonded to Au and structure B with H bonded to Si was searched by the LST/QST method. Fig. 3 shows the reaction path from structure A to B, for which there is a single TS with only one imaginary frequency of 327.3i cm^{-1}. In the TS, the Si\\H and Au\\H bond lengths are 1.69 Å and 1.90 Å, respectively. The energy barrier of 0.327 eV is relatively low and the reaction is exo-thermic with a large reaction energy of 0.588 eV. H migration from structure A to B will occur rapidly at moderate temperatures unlike the reverse reaction. Therefore, it should be possible to form the HSA structure by hydrogen termination of 12 Si atoms on the $Si_{12}Au_{20}$ cluster.
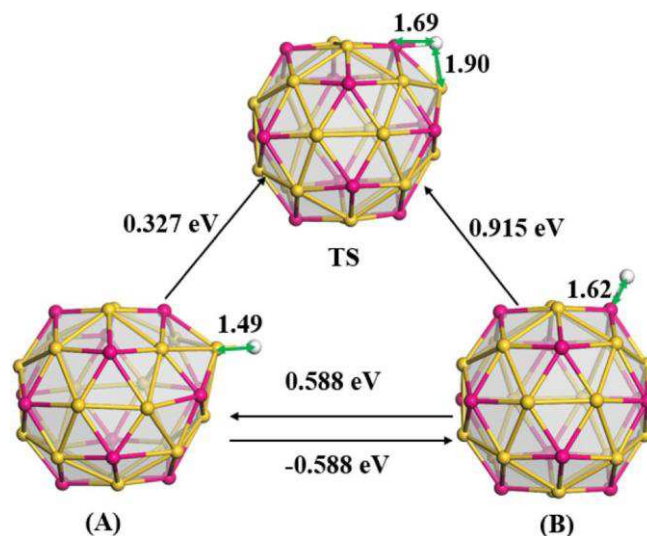

Fig. 3. Reaction path from the structure (A) formed by H atom bonded with Au atom to the structure (B) formed by H atom bonded with Si atom for H atom on the $Si_{12}Au_{20}$. The bond lengths (shown in green arrowed line) are given in Å.
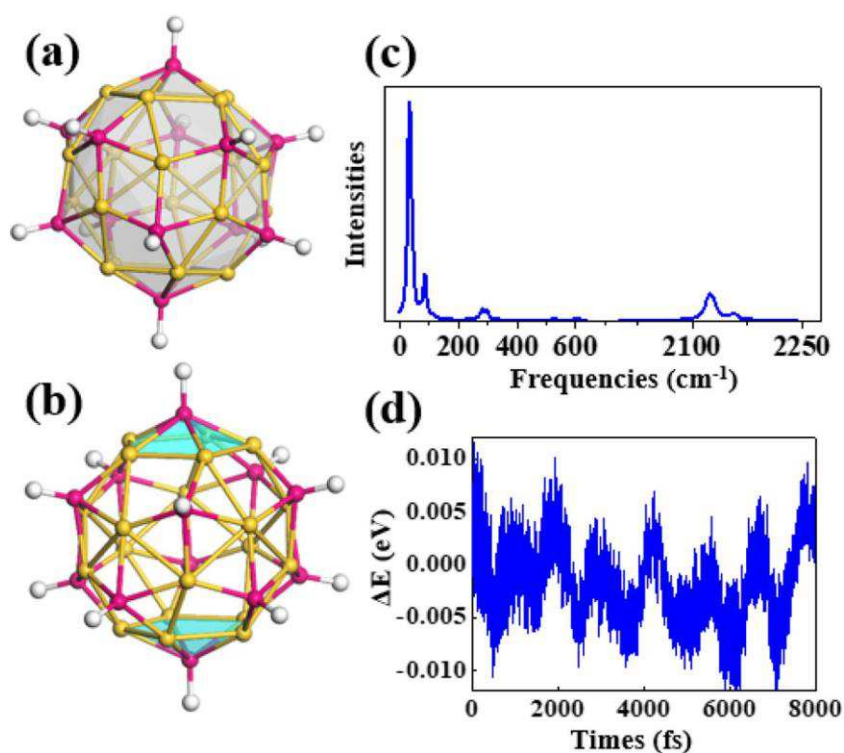
Fig. 4. (a) and (b) the optimized structure of the HSA. (c) Raman spectrum of the HSA. The temperature is 300 K and the incident light is 488.0 nm. The Lorentzian smearing is set to be 12.00 cm^{-1}. (d) Variation in the relative total energy (E) of the HSA structure as a function of time at T = 300 K.

The optimized configuration of HSA is shown in Fig. 4a and b, and with cohesive energy, bond lengths, symmetry and HOMO-LUMO gap given in Table 3, meanwhile its Cartesian coordinates are shown in Table S1 of Supplementary Information. The structure of the pure $Si_{12}Au_{20}$ cluster as shown in Fig. 1a can be viewed as the composition of 12 Au pentagons with a Si atom at the hollow centre of each Au pentagon [41], and the average lengths of Au\\Au bonds and Au\\Si bonds are 2.76 Å and 2.57 Å, respectively. However, for the structure of the HSA, we found that only two Au pentagons with the Si atom at the centre of each pentagon (referred to as $SiAu_5$ unit), as shown in green-filled areas in Fig. 4b, retain the same shape as in the pure $Si_{12}Au_{20}$ cluster, while the others have structural deformations. The av-erage lengths of Au\\Au bonds and Au\\Si bonds in the $SiAu_5$ unit are 2.74 Å and 2.59 Å, respectively, close to these of the pure $Si_{12}Au_{20}$ clus-ter. On the contrary, the average lengths of Au\\Au bonds and Au\\Si bonds in the other areas (i.e. not in the green filled areas as in Fig. 4b), are 2.83 Å and 2.49 Å, respectively. The increased Au\\Au bond lengths and the decreased Au\\Si bond lengths further show that the Si\\Au bonds has significant polarity [41]. The average length of the Si\\H bonds in the structure of HSA is 1.50 Å, which is much smaller than the value of 1.62 Å for one H atom on the $Si_{12}Au_{20}$ cluster, but consistent with previous work on hydrogenated Si-based clusters [56,57]. Because of these features, HSA has a high symmetry of S_{10}.

Next the stability of HSA was checked firstly by vibrational fre-quency analysis. We calculated the whole vibrational spectrum, but

just showed the Raman spectrum in Fig. 4c. It is noted that there is no frequency in the range of 650–2000 cm^{-1}. It can be seen from the Raman spectrum that there is no imaginary frequency, indicating the stability of the cluster. The highest frequency is 2159.79 cm^{-1} as shown in Fig. S4h (Supplementary Information), which relates to the vi-bration modes of the top H atom in the $SiAu_5$ unit as shown in Fig. 4b. Moreover, the high frequencies in the range of over 2000 cm^{-1} all relate to the vibration modes of the H atoms (see Fig. S4). These results sug-gest that the structures of $Si_{12}Au_{20}$ and $H_{12}Si_{12}Au_{20}$ can be easily charac-terized by the Raman spectra. To explore further the dynamical behaviour and thermal stability of HSA, the first-principles BOMD sim-ulation and phonon dispersion were carried out. We set a simulation time of 8 ps with a time step of 1 fs, and the structural changes were cal-culated at a constant temperature of 300 K. Fig. 4d shows how the ener-gies of the structure vary during the simulations. The total energies of HSA during the simulations remain close to constant at −209,903 eV within a very small range of variations (no N0.015 eV), strongly supporting the stability of the HSA structure at the temperature of 300 K. There is no imaginary frequency found for the HSA structure as shown in Fig. S2b (Supplementary Information), which is obtained by calculating the phonon dispersions, indicating its dynamical stability. Furthermore, the HOMO-LUMO gap of HSA is as large at 0.967 eV, just

a little smaller (by 0.071 eV) than that of the $Si_{12}Au_{20}$ cluster (1.038 eV), which indicates that the HSA structure is chemically stable. Therefore, the vibrational frequency analysis, MD simulation, phonon dispersions and electronic properties show that the HSA structure is mechanically, thermodynamically and chemically stable at the temper-ature of 300 K, which is the first step for its potential application in gas sensors.

3.4. Applications of HSA as a sensor for NH₃ and NO detection

Due to the high stability of the HSA structure, we next explored its application as a gas sensor for NH_3 and NO detection, mainly concerning the effect of hydrogenation on enhancing the gas sensing performance.

Table 3
Cohesive energy (Ec), symmetry (S), the average bond lengths (DAu-Au, DSi\Au, and DSi\H), and HOMO-LUMO gap of the $H_{12}Si_{12}Au_{20}$ cluster (HSA).

System	Ec (eV)	S	DAu-Au (Å)[a]	DSi-Au (Å)[a]	DSi-H (Å)	Eg (eV)
HSA	135.977	S_{10}	2.74/2.83	2.59/2.49	1.50	0.967

a The front values correspond to the bond lengths coming from the two $SiAu_5$ units as green-filled areas as shown in Fig. 3b, while the back values correspond to the bond lengths coming from the rest areas.

The aim of hydrogenation is to reduce the interaction between mole-cules and the Si atoms and to obtain the most stable configurations of molecules on the HSA structure, we considered all possible kinds of ini-tial structure. The optimized structures of NH₃ and NO on HSA are shown in Fig. 5, and the corresponding results are summarized in Table 4. As we expected, we found that the stable configurations of NH₃ and NO molecules on the HSA structure are formed with the N atom bonded with Au atoms (see Fig. 5). More importantly, as shown in Fig. 5a and c, the most stable adsorption sites (i.e. the Au atoms) are located in the $SiAu_5$ units. For the most stable configuration of NH₃ on the HSA, we found that the length of the N\\Au covalent bond is 2.47 Å, larger by 0.11 Å than that of NH₃ on the $Si_{12}Au_{20}$ cluster, which indi-cates a lower adsorption strength, which is consistent with the calcula-tion of adsorption energy. The most stable configuration has an adsorption energy of −0.591 eV, much smaller than that of NH₃ on the $Si_{12}Au_{20}$ cluster. However, when the NH₃ molecule adsorbs on other Au atoms as shown in Fig. 5b, it can also form a low-lying energy config-uration with an adsorption energy of −0.542 eV and with the N\\Au bond length of 2.55 Å. From the deformation electron density as shown in Fig. S5a (Supplementary Information), we conclude that there is an apparent charge transfer (at least 0.15 e) from the HSA struc-ture to the NH₃ molecule, and the HOMO-LUMO gap has been modified from the 0.967 eV in HSA to 0.937 eV and 0.925 eV for the isomer NH₃-HSA-1 and NH₃-HSA-2, respectively. These results show that the elec-tronic properties of the HSA structure are influenced by the NH₃ adsorp-tion, although the change in the gap is small.

For the NO adsorption on the HSA structure, the most stable config-uration has an adsorption energy of −0.447 eV, much smaller than that of NO adsorption on $Si_{12}Au_{20}$ cluster, and the Au\\N bond length is

Table 4
Calculated adsorption energy (E_{ads}), charge transfer from the HSA structure to molecules (E_T), the distances between the HSA and molecules (D), the HOMO-LUMO gap (E_g), and the recovery time (τ) for the configurations of NH₃ and NO adsorption on the HSA.

System	E_{ads} (eV)	E_T (e)	D (Å)	E_g (eV)	τ (s)
NH₃-HSA-1	−0.591	0.180	2.47	0.937	7.4×10^{-3}
NH₃-HSA-2	−0.542	0.152	2.55	0.925	1.1×10^{-3}
NO-HSA-1	−0.447	−0.022	2.18	0.342	2.9×10^{-5}
NO-HSA-2	−0.288	−0.017	2.53	0.237	6.5×10^{-8}

2.18 Å. The adsorption strength is further decreased when the NO mol-ecule adsorbs on the Au atoms that are not in the $SiAu_5$ units (see Fig. 5d). In this case, the adsorption energy is just −0.288 eV, which is smaller by 0.159 eV than that of the most stable configuration. Appre-ciable charge (about 0.017− 0.022 e) is found to be transferred from the NO molecule to the HSA structure, which can also be seen from the deformation electron density as shown in Fig. S5b (Supplementary Information). We note that the charges are obtained using the Hirshfeld method, which gives the smallest charge values compared with other schemes [60]. Although the HSA structure is nonmagnetic, after the ad-sorption of the NO molecule, there is about 1 μ_B magnetic moment gen-erating from the configuration of NO-HSA systems, which is similar to the case of NO molecule on the $Si_{12}Au_{20}$ cluster. More importantly, the HOMO-LUMO gaps of NO-HSA systems are in the range of 0.237−0.342 eV, compared with 0.967 eV in HSA indicating that the electronic properties of the HSA structure are substantially changed by the adsorption of NO. Similar to the case of NH₃ and NO adsorbed on the pure $Si_{12}Au_{20}$ cluster, the adsorption of NH₃ and NO induces some impurity states near the Fermi level, which leads to the narrow of

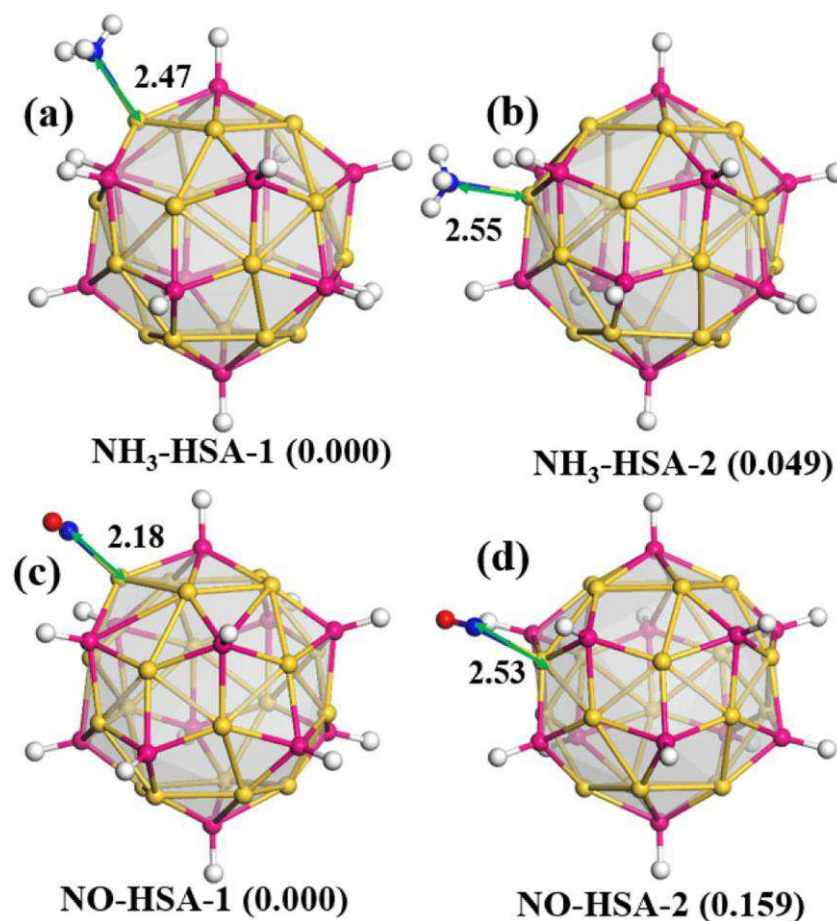Fig. 5. The optimized structures of $H_{12}Si_{12}Au_{20}$ cluster (HSA) with gas molecules adsorption: (a) and (b) NH₃; (c) and (d) NO. Values in parentheses are relative energies with respect to the most stable isomer for each adsorption in eV. The distances between molecules and cluster (shown in green arrowed line) are given in Å.

Table 5

Calculated adsorption energy per molecule (E_{ads}), charge transfer per molecule from the HSA to molecules (E_T), the average distances between the HSA and molecules (D), and the HOMO-LUMO gap (E_g) for the most stable configurations of more NO (NH_3) molecules adsorption on the HSA.

System		E_{ads} (eV)	E_T (e)	D (Å)	E_g (eV)
Species	Number of molecules				
NO	2	−0.411	−0.017	2.24	0.279
	3	−0.455	−0.027	2.19	0.183
	4	−0.463	−0.017	2.15	0.248
	5	−0.511	−0.026	2.38	0.156
	6	−0.365	−0.016	2.37	0.209
NH_3	2	−0.573	0.170	2.47	0.879
	3	−0.552	0.162	2.48	0.907
	4	−0.533	0.149	2.52	0.864
	5	−0.527	0.146	2.51	0.817
	6	−0.504	0.132	2.56	0.783

HOMO-LUMO gap (See Fig. S6 of Supplementary Information). Overall, we can conclude that the hydrogenation of the $Si_{12}Au_{20}$ cluster makes the adsorption strength decrease, which will assist the development of $Si_{12}Au_{20}$-based gas sensor with high performance.

We now discuss the gas sensing properties of the HSA-based sensor. The stability of the HSA structure has been shown above, and the ad-sorption of NO and NH_3 molecules on the HSA structure induce little de-formation of the structure, further indicating its stability. The sensitivity of the HSA-based sensor is evaluated by calculating the change of elec-tric conductivity via Eq. (2). The HOMO-LUMO gaps for the configura-tions of NH_3 (NO) molecule on the HSA structure are reduced in the range of 3.1%~4.4% (64.6%~75.5%) compared with that of the HSA struc-ture, thus leading to an increase in the electric conductivity after the ad-sorption of the NH_3 (NO) molecule. We note that the change of HOMO-LUMO gap for NH_3 adsorption is much smaller compared with that due to NO adsorption, but we confirm that it should indeed result in the change of electric conductivity, which is similar to NH_3 adsorption on the B_{40} fullerene [15,16], monolayer GaN [61,62], atomic-layer MoS_2 [63], phosphorene [64], and monolayer Ti_2CO_2 [65]. Although the ad-sorption of NH_3 on these materials does not have a substantial effect on the electronic structures of these materials, the electric conductivity of these system changes obviously after the adsorption of NH_3 owing to the comparatively large charge transfer, that is to say, the adsorption-induced charge transfer affects the resistivity of the system. For exam-ple, Moradi et al. found that the change of HOMO-LUMO gap for the most stable configuration of NH_3 adsorption on B_{40} is about 7%, which

is small but would have a significant increase of electric conductivity [16]. This conclusion is demonstrated by Lin et al. [15] who have found that the adsorption of NH_3 distinctly affect the electric conductiv-ity of the B_{40} using NEGF method. We would therefore expect a detect-able change in conductivity due to NH_3 and a large change due to NO.

To demonstrate the high selectivity of HSA for NH_3 and NO detec-tion, the adsorption behaviour of the HSA structure with CH_4, CO_2, H_2, N_2, H_2O, and O_2 are calculated, and the most stable configuration of each molecule on the HSA is shown in Fig. S7 (Supplementary Informa-tion), and the corresponding results are shown in Table S2 (Supplemen-tary Information). We found that all these molecules are physisorbed on HSA, and there is virtually no influence on the electronic properties of HSA because of the molecular adsorption, which can also be found in the DOS as shown in Fig. S6 (Supplementary Information). These results conclude that these adsorptions have negligible effect on the electric conductivity of HSA. Therefore, it is expected that HSA show high selec-tivity to distinguish NO and NH_3 from CH_4, CO_2, H_2, N_2, O_2, and H_2O gases. Furthermore, we can use the change of magnetic properties be-fore and after adsorption to differentiate between NO and NH_3. The pure HSA is nonmagnetic. The adsorption of NO introduces spin polari-zation in HSA with a magnetic moment of 1 μ_B, but the net spin polari-zation of HSA is not modified due to the adsorption of NH_3. Finally, the recovery time can be calculated using Formula (3). Since the hydroge-nated strategy has clearly decreased the adsorption strength of NH_3 and NO on the HSA structure, the recovery time is expected to be shorter. We have calculated the recovery times at the temperature of 300 K, which are summarized in Table 4. For most stable adsorption states of NH_3 and NO, the recovery time is estimated to be about 7.4 ms and 29 μs, respectively, which indicates high performance for the HSA-based gas sensor. Therefore, we conclude that HSA may show high performance as a gas sensor, including high stability, sensitivity, selectivity and a short recovery time for NH_3 and NO detection.

We further considered several NO and NH_3 molecules adsorbed on HSA to explore the coverage effect. In order to explore a range of differ-ent coverages, up to six molecules and several different starting config-urations were investigated. The structural, energetic, and electronic properties of the most stable configurations for these systems are pre-sented in Table 5 and Fig. 6. After the addition of each molecule, the sys-tem is geometry optimized prior to the addition of the subsequent molecule. Although interestingly, the most stable configuration for $5NH_3$@HSA could only be generated from the second most stable con-figuration of $4NH_3$@HSA; however, we note that the energy difference between the first and second most stable configurations of $4NH_3$@HSA is very small (only 0.008 eV). For No adsorption we find that, the second
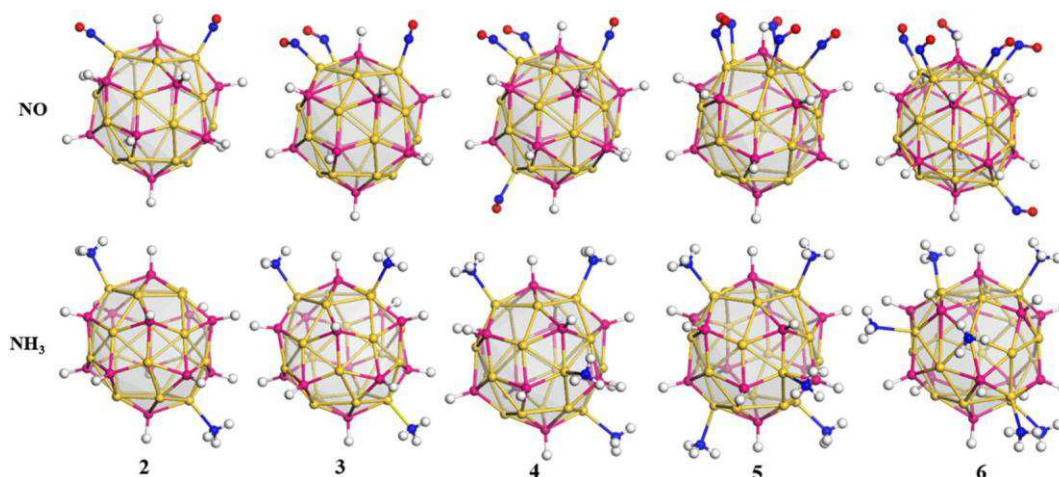

Fig. 6. The optimized structures of $H_{12}Si_{12}Au_{20}$ cluster (HSA) adsorbed by NO and NH_3 molecules of different coverage.
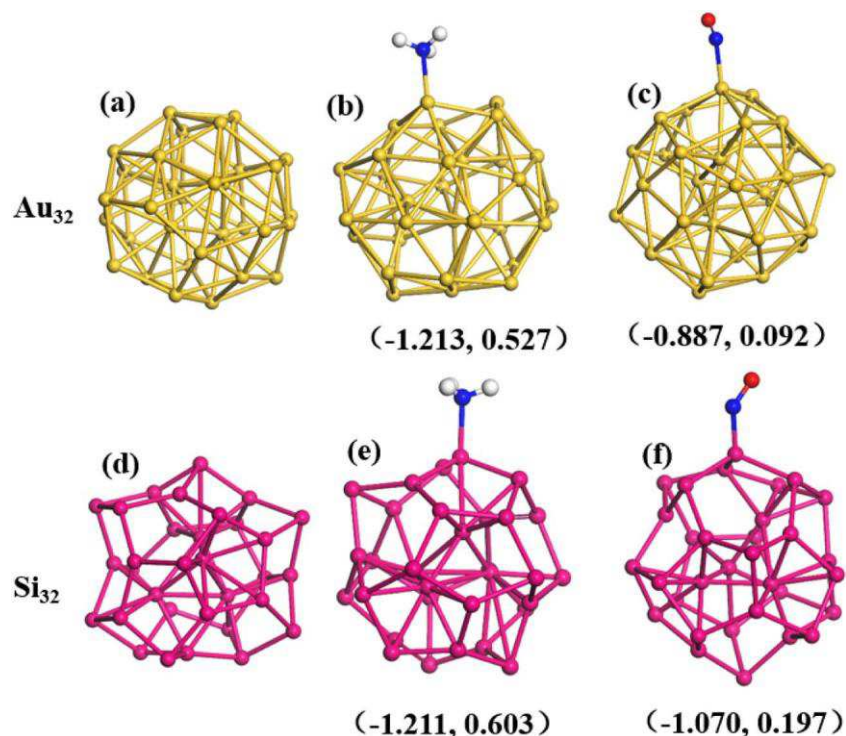
Fig. 7. The optimized structures of Au_{32} and Si_{32} clusters without and with NO and NH_3 adsorption. The values in parentheses, in turn, are adsorption energy and HOMO-LUMO gap.

configuration for four NO molecules are all located at the same $SiAu_5$ unit. Moreover, in general, for NO adsorption with different coverages, the changes of E_{ads} are very small, which is important for their use in gas sensors, while the HOMO-LUMO gaps basically are all smaller than that of one NO molecule adsorption. When the number of NO molecules reaches 6, the adsorption energy becomes much higher. For NH_3 ad-sorption, the E_{ads} and HOMO-LUMO gaps decrease as coverage increases but the variation of E_{ads} is still small. These results further indicate that HSA is a promising candidate for gas sensors with high performance for NH_3 and NO detection with low coverage.

Moreover, to have comprehensive and comparable studies on the gas sensing properties of NO and NH_3 molecules adsorbed on the (hydrogenated) $Si_{12}Au_{20}$ cluster, we also calculated the adsorption of NO and NH_3 molecules on the Au_{32} and Si_{32} clusters, which have the same size as $Si_{12}Au_{20}$ cluster. Although the Au_{32} cluster with I_h icosahedral symmetry is the most stable structure at zero temperature, experimen-tal and theoretical studies have found that its amorphous isomer with C_1 symmetry becomes the most stable above 300 K [66–68]. In general, we aim for a gas sensor that can be used at room or higher temperatures, thus, in the present work, we only considered the most stable structure of Au_{32} cluster above 300 K. The most stable structure of the Si_{32} cluster can be viewed as endohedral fullerene (i.e. $Si_4@Si_{28}$) [69,70]. After the relaxation of NO and NH_3 molecules on the Au_{32} and Si_{32} clusters, the results are shown in Fig. 7. It is found that the adsorption energies of both NO and NH_3 on the Au_{32} and Si_{32} clusters are much bigger (at least −0.887 eV). These adsorption energies are so large that the recov-ery times of both clusters would be long. For example, the adsorption energies of NO on the Au_{32} cluster is −0.887 eV, which corresponds to a recovery time of about 10 min, while the others correspond too much longer recovery times (over hours). As discussed above, long re-covery times will impede the reuse of gas sensors. Moreover, previous studies indicated that the adsorption energies of CO and O_2 molecules on the Au_{32} cluster are all larger than −1 eV [68], indicating that the se-lectivity of the Au_{32} cluster is not good. Therefore, from the viewpoint of stability, recovery time and selectivity, the pure Au_{32} and Si_{32} clusters are not suitable candidates for gas sensors for detecting NO and NH_3.

4. Summary and conclusions

Using DFT techniques, we have investigated the adsorption behav-iour and electronic properties of NH_3, NO, CH_4, CO_2, H_2, N_2, O_2, and H_2O molecules on the (hydrogenated) $Si_{12}Au_{20}$ cluster in order to find a promising molecular sensor for NH_3 and NO detection. NH_3 and NO are chemisorbed on the $Si_{12}Au_{20}$ cluster with a large adsorption energy and apparent charge transfer, while the other molecules are all physisorbed on the cluster. The electronic properties of the $Si_{12}Au_{20}$ cluster change dramatically due to the adsorption of NH_3 and NO mole-cules, particularly regarding the electric conductivity. Our results sug-gest that the $Si_{12}Au_{20}$-based sensor could show high sensitivity and selectivity; however, because of the strong adsorption of NH_3 and NO molecules, the $Si_{12}Au_{20}$-based sensor would suffer a longer recovery time (over 3 h), which directly prevents its application in gas sensors. To improve the recovery time, we then explored the hydrogenation of Si atoms in the $Si_{12}Au_{20}$ cluster due to the strong adsorption occurring in the interaction between the molecules and the Si atoms. The struc-ture, stability and electronic properties of the hydrogenated $Si_{12}Au_{20}$ cluster ($H_{12}Si_{12}Au_{20}$, i.e. HSA) were investigated. The vibrational fre-quency analysis, MD simulation and electronic properties showed that the HSA structure is mechanically, thermodynamically and chemically stable at T = 300 K. We found that the adsorption strength of NH_3 and NO on the HSA is moderate and much smaller than that of NH_3 and NO on the $Si_{12}Au_{20}$ cluster. The other molecules considered are still physisorbed on the HSA, and have a negligible effect on the elec-tronic properties of material. For NH_3 and NO, the recovery time of the HSA is predicted to be 7.4 ms and 29 μs, respectively. We also consid-ered two to six NO or NH_3 molecules adsorbed on HSA, corresponding to different coverage, and the adsorption of NO and NH_3 on the Au_{32} and Si_{32} clusters, respectively.

Overall, we conclude that due to the moderate adsorption energy, clear charge transfer, significant change of electric conductivity, and very short recovery time, HSA can be viewed as a promising gas sen-sor with high performance for NH_3 and NO detection at low coverage.

Declaration of Competing Interest

There are no conflicts of interest to declare.

Acknowledgements

Appendix A. Supplementary data

Additional data and figures related to the deformation electronic densities of the $Si_{12}Au_{20}$ and $H_{12}Si_{12}Au_{20}$ cluster with NH_3 and NO; the frequency modes of $H_{12}Si_{12}Au_{20}$ cluster; The stable configurations of common molecules on the $H_{12}Si_{12}Au_{20}$ and the corresponding results (PDF).

References

[1] X. Liang, Z. Chen, H. Wu, L. Guo, C. He, B. Wang, Y. Wu, Enhanced NH_3-sensing behavior of 2,9,16,23-tetrakis (2,2,3,3-tetrafluoropropoxy) metal(II) phthalocyanine/ multi-walled carbon nanotube hybrids: an investigation of the effects of central metals, Carbon 80 (2014) 268−278.

[2] R. Chandiramouli, A. Srivastava, V. Nagarajan, NO adsorption studies on silicene nanosheet: DFT investigation, Appl. Surf. Sci. 351 (2015) 662−672.

[3] R. Ferrando, J. Jellinek, R.L. Johnston, Nanoalloys: from theory to applications of alloy clusters and nanoparticles, Chem. Rev. 108 (2008) 845−910.

[4] T. Zhao, T. Zhou, Q. Yao, C. Hao, X. Chen, Metal nanoclusters: applications in environmental monitoring and cancer therapy, J. Environ. Sci. Health C Environ. Carcinog. Ecotoxicol. Rev. 33 (2015) 168−187.

[5] Y. Yong, C. Li, X. Li, T. Li, H. Cui, S. Lv, Ag_7Au_6 cluster as a potential gas sensor for CO, HCN, and NO detection, J. Phys. Chem. C 119 (2015) 7534−7540.

[6] J. van Lith, A. Lassesson, S.A. Brown, M. Schulze, J.G. Partridge, A. Ayesh, Hydrogen sensor based on tunneling between palladium clusters, Appl. Phys. Lett. 91 (2007), 181910.

[7] Y. Yong, X. Li, T. Li, H. Cui, S. Lv, $W@Si_{12}$ cluster as a potential sensor for CO and NO detection, Europhys. Lett. 111 (2015), 10006.

[8] K. Suematsu, Y. Shin, Z. Hua, K. Yoshida, M. Yuasa, T. Kida, K. Shimanoe, Controlled clustering of SnO_2 nanoparticles for highly sensitive toluene detection, ACS Appl. Mater. Interfaces 6 (2015) 5319−5326.

[9] X. Liu, N. Chen, B. Han, X. Xiao, G. Chen, I. Djerdj, Y. Wang, Nanoparticle cluster gas sensor: Pt activated SnO_2 nanoparticles for NH_3 detection with ultrahigh sensitivity, Nanoscale 7 (2015) 14872−14880.

[10] A. Soltani, S.G. Raz, M.R. Taghartapeh, A.V. Moradi, R.Z. Mehrabian, Ab initio study of the NO_2 and SO_2 adsorption on $Al_{12}N_{12}$ nano-cage sensitized with gallium and magnesium, Comput. Mater. Sci. 79 (2013) 795−803.

[11] J. Beheshtian, A.A. Peyghan, Z. Bagheri, Selective function of $Al_{12}N_{12}$ nano-cage towards NO and CO molecules, Comput. Mater. Sci. 62 (2012) 71−74.

[12] Y. Yong, X. Li, Q. Zhou, X. Su, T. Li, H. Cui, S. Lv, Adsorption of gas molecules on $Gd@Au_n$ (n=14,15) clusters and their implication for molecule sensors, RSC Adv. 6 (2016) 26809−26816.

[13] H. Cui, Y. Yong, H. Jiang, L. Yang, S. Wang, G. Zhang, M. Guo, X. Li, The $M_{12}N_{12}$ (M= Al, Ga) clusters as potential sensors for NO, NO_2 and HCN detection, Mater. Res. Ex-press 4 (2017), 015009.

[14] Y. Yong, S. Lv, R. Zhang, Q. Zhou, X. Su, T. Li, H. Cui, $C_{54}Si_6$ heterofullerene as a poten-tial gas sensor for CO, NO, and HCN detection, RSC Adv. 6 (2016) 89080−89088.

[15] B. Lin, H. Dong, C. Du, T. Hou, H. Lin, Y. Li, B_{40} fullerene as a highly sensitive molecular device for NH_3 detection at low bias: a first principles study, Nanotechnology 27 (2016), 075501.

[16] M. Moradi, V. Vahabi, A. Bodaghi, Computational study on the fullerene-like B_{40} borosphere properties and its interaction with ammonia, J. Mol. Liq. 223 (2016) 315−320.

[17] A.I. Ayesh, Metal/metal-oxide nanoclusters for gas sensor applications, J. Nanomater. 2016 (2016), 2359019.

[18] Y. Yong, Y. Su, Y. Kuang, X. Li, Z. Lu, B_{40} and $M@B_{40}$ (M=Li and Ba) fullerenes as po-tential molecular sensors for acetone detection: a first-principles study, J. Mol. Liq. 264 (2018) 1−8.

[19] N.L. Hadipour, A.A. Peyghan, H. Soleymanabadi, Theoretical study on the Al-doped ZnO nanoclusters for CO chemical sensors, J. Phys. Chem. C 119 (2015) 6398−6404.

[20] Y. Yong, H. Jiang, X. Li, S. Lv, J. Cao, The cluster-assembled nanowires based on $M_{12}N_{12}$ (M = Al and Ga) clusters as potential gas sensors for CO, NO, and NO_2 de-tection, Phys. Chem. Chem. Phys. 18 (2016) 21431−21441.

[21] A. Mathew, T. Pradeep, Noble metal clusters: applications in energy, environment, and biology, Part. Part. Syst. Charact. 31 (2014) 1017−1053.

[22] Y. Yong, X. Su, Q. Zhou, Y. Kuang, X. Li, The $Zn_{12}O_{12}$ cluster-assembled nanowires as a highly sensitive and selective gas sensor for NO and NO_2, Sci. Rep. 7 (2017), 17505.

[23] Y. Tang, B. Su, M. Liu, Y. Feng, X. Jiang, L. Jiang, A. Yu, Superwettability strategy: 1D assembly of binary nanoparticles as gas sensors, Small 13 (2017), 1601087.

[24] S. Li, J. Qiu, M. Ling, F. Peng, B. Wood, S. Zhang, Photoelectrochemical characterization of hydrogenated TiO_2 nanotubes as photoanodes for sensing applications, ACS Appl. Mater. Interfaces 5 (2013) 11129−11135.

[25] X. Yan, L. Tian, X. Tan, M. Zhou, L. Liu, X. Chen, Modifying oxide nanomaterials' prop-erties by hydrogenation, MRS Commun. 6 (2016) 192−203.

[26] M. Wang, Y. Wang, J. Liu, C. Pei, B. Liu, Y. Yuan, H. Zhao, S. Liu, H. Yang, Enhanced sensing performance and sensing mechanism of hydrogenated NiO particles, Sen-sors Actuators B 250 (2017) 208−214.

[27] Y. Wang, J. Liu, M. Wang, C. Pei, B. Liu, Y. Yuan, S. Liu, H. Yang, Enhancing the sensing properties of TiO_2 nanosheets with exposed {001} facets by a hydrogenation and sensing mechanism, Inorg. Chem. 56 (2017) 1504−1510.

[28] J. Wang, Y. Liu, Y. Li, Growth behavior, stability and electronic structure, Phys. Lett. A 374 (2010) 2736−2742.

[29] W. Ma, F. Chen, Electronic, magnetic and optical properties of Cu, Ag, Au-doped Si clusters, J. Mol. Model. 19 (2013) 4555−4560.

[30] S. Lu, X. Xu, G. Feng, H. Xu, W. Zheng, Structural and electronic properties of $AuSi_n^-$ (n = 4−12) clusters: photoelectron spectroscopy and ab initio calculations, J. Phys. Chem. C 120 (2016) 25628−25637.

[31] Y. Li, J.T. Lyon, A.P. Woodham, P. Lievens, A. Fielicke, E. Janssens, Structural identifi-cation of gold-doped silicon clusters via far-infrared spectroscopy, J. Phys. Chem. C 119 (2015) 10896−10903.

[32] N. Uchida, T. Miyazaki, T. Kanayama, Stabilization mechanism of Si_{12} cage clusters by encapsulation of a transition-metal atom: a density-functional theory study, Phys. Rev. B 74 (2006), 205427.

[33] Y. Li, A. Mao, Y. Li, X. Kuang, Density functional study on size-dependent structures, stabilities, electronic and magnetic properties of Au_nM (M=Al and Si, n=1−9) clus-ters: comparison with pure gold clusters, J. Mol. Model. 18 (2012) 3061−3072.

[34] K. Joshi, S. Krishnamurty, Thermo-stimuli response of doped MAu_n^- clusters (n = 4 −8; M = Si, Ge) at discrete temperatures: a BOMD undertaking, J. Phys. Chem. C 121 (2017) 17514−17522.

[35] K. Majer, B.V. Issendorff, Photoelectron spectroscopy of silicon doped gold and silver cluster anions, Phys. Chem. Chem. Phys. 14 (2012) 9371−9376.

[36] H. Wang, W. Lu, L. Zhao, W. Qin, W. Yang, X. Xue, Structures and electronic properties of the $SiAu_n$ (n=17−20) clusters, J. Phys. Chem. A 117 (2013) 2672−2677.

[37] D. Manzoor, S. Krishnamurty, S. Pal, Effect of silicon doping on the reactivity and cat-alytic activity of gold clusters, J. Phys. Chem. C 118 (2014) 7501−7507.

[38] P. Ranjan, A. Kumar, T. Chakraborty, Computational study of Au_mSi_n (mn= 2-6) nanoalloy clusters invoking density functional based descriptors, J. Phys. Conf. Ser. 759 (2016), 012045.

[39] P. Ranjan, A. Kumar, T. Chakraborty, Theoretical analysis: electronic and optical properties of gold silicon nanoalloy clusters, Mater. Today Proc. 3 (2016) 1563−1568.

[40] S. Gautam, N. Goel, K. Dharamvir, A DFT based prediction of gold fullerene $Au_{92}Si_{12}$ with the aid of silicon, RSC Adv. 4 (2014) 13927−13933.

[41] J.J. Guo, H.Y. Zhao, J. Wang, L.Y. Ai, Y. Liu, $Au_{20}Si_{12}$: a hollow catalan pentakis dodeca-hedron, J. Chem. Phys. 146 (2017), 064310.

[42] H. Zhao, J. Wang, L. Ai, Y. Liu, $Cu_{20}Si_{12}$: a hollow cage constituted of a copper dodeca-hedron and a silicon icosahedron, J. Phys. Chem. A 120 (2016) 6303−6308.

[43] B. Delley, An all-electron numerical method for solving the local density functional for polyatomic molecules, J. Chem. Phys. 92 (1990) 508−517.

[44] B. Delley, From molecules to solids with the $DMol^3$ approach, J. Chem. Phys. 113 (2000) 7756−7764.

[45] J.P. Perdew, K. Burke, M. Ernzerhof, Generalized gradient approximation made sim-ple, Phys. Rev. Lett. 77 (1996) 3865−3868.

[46] A. Tkatchenko, M. Scheffler, Accurate molecular van der Waals interactions from ground-state electron density and free-atom reference data, Phys. Rev. Lett. 102 (2009), 073005.

[47] D.R. Hamann, M. Schluter, C. Chiang, Norm-conserving pseudopotentials, Phys. Rev. 43 (1979) 1494−1497.

[48] F.L. Hirshfeld, Bonded-atom fragments for describing molecular charge densities, Theor. Chim. Acta 44 (1977) 129−138.

[49] N. Govind, M. Petersen, G. Fitzgerald, D. King-Smith, J. Andzelm, A generalized syn-chronous transit method for transition state location, Comput. Mater. Sci. 28 (2003) 250−258.

[50] W. Hu, N. Xia, X. Wu, Z. Li, J. Yang, Silicene as a highly sensitive molecule sensor for NH_3, NO and NO_2, Phys. Chem. Chem. Phys. 16 (2014) 6957−6962.

[51] S.T. Bromley, M.A. Zwijnenburg, T. Maschmeyer, Fully coordinated silica nanoclusters: $(SiO_2)_N$ molecular rings, Phys. Rev. Lett. 90 (2003), 035502.

[52] A.C. Filippou, B. Baars, O. Chernov, Y.N. Lebedev, G. Schnakenburg, Silicon−oxygen double bonds: a stable silanone with a trigonal-planar coordinated silicon center, Angew. Chem. Int. Ed. 53 (2014) 565−570.

[53] A. El-Sayed, M.B. Watkins, T. Grasser, V.V. Afanasev, A.L. Shluger, Hydrogen-induced rupture of strained Si-O bonds in amorphous silicon dioxide, Phys. Rev. Lett. 114 (2015), 115503.

[54] S. Peng, K. Cho, P. Qi, H. Dai, Ab initio study of CNT NO_2 gas sensor, Chem. Lett. 387 (2004) 271−276.

[55] D. Palagin, K. Reuter, Evaluation of endohedral doping of hydrogenated Si fullerenes as a route to magnetic Si building blocks, Phys. Rev. B 86 (2012), 045416.

[56] Y. Yong, Q. Zhou, X. Li, S. Lv, The $H_{60}Si_6C_{54}$ heterofullerene as high-capacity hydro-gen storage medium, AIP Adv. 6 (2016), 07532.

[57] V. Kumar, Y. Kawazoe, Hydrogenated silicon fullerenes: effects of H on the stability of metal-encapsulated silicon clusters, Phys. Rev. Lett. 90 (2003), 055502.

[58] J. Jia, Y. Lai, H. Wu, H. Jiao, Structure and stability of tube and cage $(SiH)_{60}$, J. Phys. Chem. C 113 (2009) 6887−6890.

[59] F. Marsusi, M. Qasemnazhand, Sila-fulleranes: promising chemically active fullerene analogs, Nanotechnology 27 (2016), 275704.

[60] E.R. Davidson, S.A. Chakravorty, Test of the Hirshfeld definition of atomic charges and moments, Theor. Chim. Acta 83 (1992) 319−330.

[61] Y. Yong, X. Su, H. Cui, Q. Zhou, Y. Kuang, X. Li, Two-dimensional tetragonal GaN as potential molecule sensors for NO and NO_2 detection: a first-principle study, ACS Omega 2 (2017) 8888−8895.

[62] Y. Yong, H. Cui, Q. Zhou, X. Su, Y. Kuang, X. Li, Adsorption of gas molecules on a graphitic GaN sheet and its implications for molecule sensors, RSC Adv. 7 (2017) 51027−51035.

[63] B. Cho, M.G. Hahm, M. Choi, J. Yoon, A.R. Kim, Y. Lee, S. Park, J. Kwon, C.S. Kim, M. Song, Y. Jeong, K. Nam, S. Lee, T.J. Yoo, C.G. Kang, B.H. Lee, H.C. Ko, P.M. Ajayan, D. Kim, Charge-transfer-based gas sensing using atomic-layer MoS_2, Sci. Rep. 5 (2015) 8052.

[64] L. Kou, T. Frauenheim, C. Chen, Phosphorene as a superior gas sensor: selective adsorption and distinct I−V response, J. Phys. Chem. Lett. 5 (2014) 2675−2681.

[65] X. Yu, Y. Li, J. Cheng, Z. Liu, Q. Li, W. Li, X. Yang, B. Xiao, Monolayer Ti_2CO_2: a prom-ising candidate for NH_3 sensor or capturer with high sensitivity and selectivity, ACS Appl. Mater. Interfaces 7 (2015) 13707−13713.

[66] M. Ji, X. Gu, X. Li, X. Gong, J. Li, L. Wang, Experimental and theoretical investigation of the electronic and geometrical structures of the Au_{32} cluster, Angew. Chem. Int. Ed. 44 (2005) 7119−7123.

[67] X. Gu, M. Ji, S.H. Wei, X.G. Gong, Au_N clusters (N=32,33,34,35): Cagelike structures of pure metal atoms, Phys. Rev. B 70 (2004), 205401.

[68] Y. Wang, X.G. Gong, First-principles study of interaction of cluster Au_{32} with CO, H_2, and O_2, J. Chem. Phys. 125 (2006), 124703.

[69] S. Yoo, N. Shao, C. Koehler, T. Fraunhaum, X.C. Zeng, Structures and relative stability of medium-sized silicon clusters. V. Low-lying endohedral fullerenelike clusters Si_{31}−Si_{40} and Si_{45}, J. Chem. Phys. 124 (2006), 164311.

[70] L. Ma, J. Zhao, J. Wang, B. Wang, G. Wang, Lowest-energy endohedral fullerene structures of Si_N (30 N 39) clusters by density functional calculations, Phys. Rev. A 73 (2006), 063203.